A Comparison of Change Detection Statistics in POLSAR Images

P. R. Kersten, J. S. Lee, T. L. Ainsworth
The Naval Research Laboratory
Remote Sensing Division, Code 7263
Washington, DC USA 20375
kersten@nrl.navy.mil

***Abstract*—Change detection in polarimetric SAR (POLSAR) images is an important topic. Three statistics are compared on both simulated and real data for their efficacy in change detection. The three statistics are the contrast ratio, the ellipticity and the Bartlett test. The relative performance for these three test statistics on the two simulations is dramatically different. The results are illustrated and explained.**

Keywords- change-detection, ellipticity, contrast ratio, Bartlett test, hypothesis test, Wishart Distribution, POLSAR images.

I. INTRODUCTION

Polarimetric SAR (POLSAR) data contains both phase and amplitude information from radar returns transmitted in two different polarizations. The active nature of POLSAR means the sensor can collect information through cloud cover or bad weather at anytime, night-or-day. Change detection in multi-temporal POLSAR images is an active area of research with applications in agriculture, resource assessment and target detection.

The remainder of this paper is organized as follows: In section II, the POLSAR model is described and in section III, the three statistics are defined and discussed. In section IV, two simulations are described, one that is statistically ideal and another based on real data where a target is embedded in one of the images. The statistics are rank-ordered on performance in both simulations and these ranks change between the ideal and real simulations. Reasons for these differences are discussed. The conclusions are contained in section V.

II. THE POLARIMETRIC SAR MODEL

POLSAR images are constructed from complex radar returns acquired from a fully-polarimetric radar system. The four possible polar combinations of transmit-receive returns of the radar are: HH, HV, VH, and VV. For example, the complex number VH represents the returned horizontally polarized signal from a vertically transmitted radar signal. The other variables are similarly defined. Under certain symmetry assumptions, the complex returns HV and VH, are identical yielding a 3-D complex scattering vector:

$$x = [HH, \sqrt{2}HV, VV]^t . \tag{1}$$

The pixel feature is the complex covariance matrix defined in (2), which is formed from the Hermitian outer product of this vector x. The resulting Hermitian positive-semidefinite matrix contains nine real independent components, which form the elements of a feature vector associated with each pixel. In practice, POLSAR images are filtered to reduce the speckle noise and ensure that covariance matrix is full rank. This filtering replaces each pixel with a weighted average of its neighboring pixels, where n is the effective number of looks or independent samples. Naively, one can think of the covariance associated with each pixel as:

$$\hat{\Sigma}_x = \frac{1}{n}\sum_{i=1}^{n} x_i x_i^{t*} . \tag{2}$$

In practice, the speckle filtering plays an important role in the efficacy of the change detection. In this paper, a 5x5 speckle filter [1] was used to filter the pair of real images and a 5x5 Box Filter was used to filter the statistically ideal images.

The sample covariance has the complex Wishart distribution if one assumes the components of x_i are complex Gaussian random variates. Defining, $X = n\hat{\Sigma}_x = \sum_{i=1}^{n} x_i x_i^{t*}$ then $X \sim W_C(p, n, \Sigma_x)$ where the distribution is defined as:

$$W_C(p, n, \Sigma_x) = \frac{|X|^{n-p}}{\Gamma_p(n)|\Sigma_x|^n}\exp(-tr[\Sigma_x^{-1}X]) \tag{3}$$

and $\Gamma_p(n) = \pi^{p(p-1)/2}\prod_{j=1}^{p}\Gamma(n-j+1)$. Thus, the pixel features of the filtered images are modeled as Wishart random variables.

III. THREE CHANGE STATISTICS

The first statistic is a generalization of the standard change of real covariance matrices derived originally by Wilks circa 1932 [2, p. 292]. Here the covariance is complex. This case was analyzed in detail in [3] and its applications studied in [4]. This likelihood ratio test (LRT) statistic is derived from the Wishart probability density function (PDF) for the α-level test. If Σ_x and Σ_y represent the pixel covariance's from the same pixel in both images, then this statistic studied here is:

$$T_b = \ln\left(|\Sigma_{avg}|/|\Sigma_x|\right) + \ln\left(|\Sigma_{avg}|/|\Sigma_y|\right) \tag{4}$$

Report Documentation Page

Form Approved
OMB No. 0704-0188

1. REPORT DATE	2. REPORT TYPE	3. DATES COVERED
25 JUL 2005	**N/A**	**-**

4. TITLE AND SUBTITLE	5a. CONTRACT NUMBER
A Comparison of Change Detection Statistics in POLSAR Images	5b. GRANT NUMBER
	5c. PROGRAM ELEMENT NUMBER
6. AUTHOR(S)	5d. PROJECT NUMBER
	5e. TASK NUMBER
	5f. WORK UNIT NUMBER
7. PERFORMING ORGANIZATION NAME(S) AND ADDRESS(ES) **The Naval Research Laboratory Remote Sensing Division, Code 7263 Washington, DC USA 20375**	8. PERFORMING ORGANIZATION REPORT NUMBER
9. SPONSORING/MONITORING AGENCY NAME(S) AND ADDRESS(ES)	10. SPONSOR/MONITOR'S ACRONYM(S)
	11. SPONSOR/MONITOR'S REPORT NUMBER(S)

12. DISTRIBUTION/AVAILABILITY STATEMENT
Approved for public release, distribution unlimited

13. SUPPLEMENTARY NOTES
See also ADM001850, 2005 IEEE International Geoscience and Remote Sensing Symposium Proceedings (25th) (IGARSS 2005) Held in Seoul, Korea on 25-29 July 2005. , The original document contains color images.

14. ABSTRACT

15. SUBJECT TERMS

16. SECURITY CLASSIFICATION OF:			17. LIMITATION OF ABSTRACT	18. NUMBER OF PAGES	19a. NAME OF RESPONSIBLE PERSON
a. REPORT **unclassified**	b. ABSTRACT **unclassified**	c. THIS PAGE **unclassified**	**UU**	**4**	

where $\Sigma_{avg} = (\Sigma_x + \Sigma_y)/2$. Intuitively, the dissimilarity (4) represents the divergence of two averaging methods - determinant of the arithmetic mean to the geometric mean of the determinants. Here this test is called the Bartlett test since he proposed the ratio of the arithmetic and geometric means of the sample variances as a robust test for the equality of two distributions - thus the name [5, p. 188]. Under the null hypothesis both images are identical, so $T_b = 0$. The rejection region is $T_b > threshold$.

The second statistic is called the Contrast Ratio and is defined using the Rayleigh Quotient. It is well known that the $\sup_x \frac{x^h \Sigma_y x}{x^h \Sigma_x x}$ is the maximum eigenvalue, say $\lambda_{\max}$, of $Cxy = (\Sigma_x^{-\frac{1}{2}})^h \Sigma_y \Sigma_x^{-\frac{1}{2}}$. It is a measure of the change between the two images' pixel covariance. So too is the inverse of the smallest eigenvalue denoted by $\lambda_{\min}^{-1}$. The images are identical under the null hypothesis, so all the eigenvalues should be one. The contrast ratio is defined as:

$$T_{cr} = \ln(\max(\lambda_{\max}, \lambda_{\min}^{-1})) \tag{5}$$

and the form of the rejection region is similar to T_b.

The third statistic is the ellipticity [2, p. 336], which is applied to the matrix Cxy. Here, one is testing if this quotient Cxy is proportional to the identity matrix. Cxy is also a positive definite Hermitian matrix since both Σ_x and Σ_y are. The form of the ellipticity applied here is given by:

$$T_e = -\ln \prod_{i=1}^{p} \lambda_i + p \ln\left(\frac{1}{p}\sum_{i=1}^{p} \lambda_i\right), \tag{6}$$

where $\lambda_i, i = 1,2,3 = p$. The rejection region is the same for this test as well.

IV. The Simulations

Two simulations were run to test the efficacy of these three statistics in detecting change between the pair of images. The first simulation generates two pairs of images, which have a sample covariance that is typical of trees – as extracted from an ESAR data set. The correlation of the background can be varied by using a convex combination of the background from one image and a second generated image with the same background. Mixed into the second image is a target covariance. These images are then just large test sets to estimate the detection probabilities for the three statistics. The second simulation involves taking a pair of multi-temporal L-Band Images that have been registered and injecting (adding) a target grid into the second image. Then the probability of error can be estimated by varying the threshold to obtain a fixed α-level test and obtaining the probability of detection on the grid of targets. In addition, the Expectation Maximization (EM) algorithm is applied to estimate the Bayes Error. These methods yield what seems to be contradictory results, in that the order of performance of these statistics is reversed. It is conjectured that the robustness of statistics to changes in the underlying distributions is the cause of this anomaly.

A. Simulated Background and Target

The first simulation is purely computer generated hypothesis test between two covariance matrices. Under the null hypothesis, the covariance matrix is representative of a group of trees. The alternative hypothesis covariance is representative of a double-bounce structure. The correlated images were created by first generating two random copies of the first image and then mixing the first image into the second random copy. This mixing coefficient used in a convex combination is a measure of the correlation and was set at 0.2, 0.5 and 0.8 to generate two images under the null hypothesis. To the correlated second image is added the target covariance as a convex combination. As the proportion of signal mixed into the second image goes from zero to one, the signal-to-noise ratio (SNR) increases from zero to its maximum value. Both images are filtered using a simple 5x5 box filter or Daniel filter since there are no topographic variations in the images. Based on the null hypothesis, the threshold for a fixed false alarm rate (alpha level) of 0.001 is determined from the data and fixed as the SNR increases from zero to its maximum value. Figure 1 contains a plot of the probability of detection versus the proportion of mixed signal.

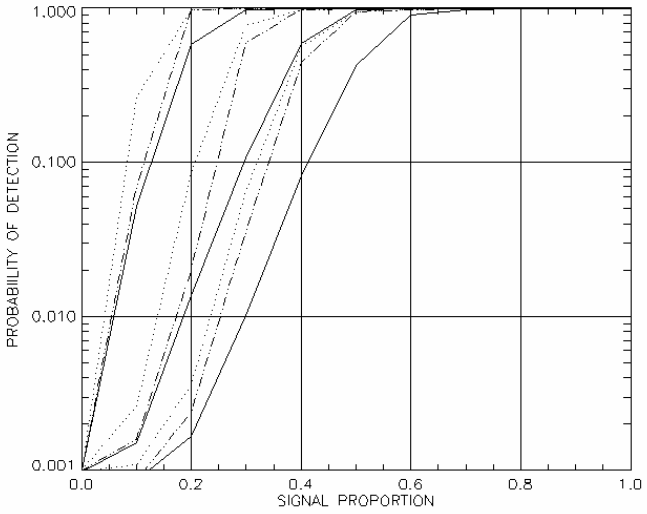

Figure 1. Probability of Detection vs proportion of signal in the second image. The dotted curve is the ellipticity, the dash-dot curve is the Bartlett and the solid curve the contrast ratio. The three sets of currves are ordered right-to-left with correlation coefficients 0.2, 0.5, 0.8.

Each of these statistics assumes that the generating mechanism results from complex Gaussian random vectors that produce the complex Wishart covariance samples. One could argue that the ellipticity is more sensitive since it is tuned to test the variation of the covariance of Cxy from the identity matrix, whereas the Bartlett only compares the equality of any two matrices. Likewise, the contrast ratio makes use of only two of the eigenvalues of Cxy and should be less sensitive to changes in the images. Although this is only an ad hoc heuristic argument, it is plausible if one ignores the robustness of these statistics to changes in the underlying assumptions and

especially the pixel-to-pixel variation in the image, which is ignored by this statistical modeling.

B. *Real Background with Injected Target*

This simulation is more realistic since it uses registered L-band repeat pass POLSAR image-pairs from the Glen Affric project [6]. A 512x512 image chip was taken from this data and into one chip, a grid of target covariance patches is added. Both images are then filtered using a 5x5 speckle filter for single look complex POLSAR images. The filtered target image is given in figure 2.

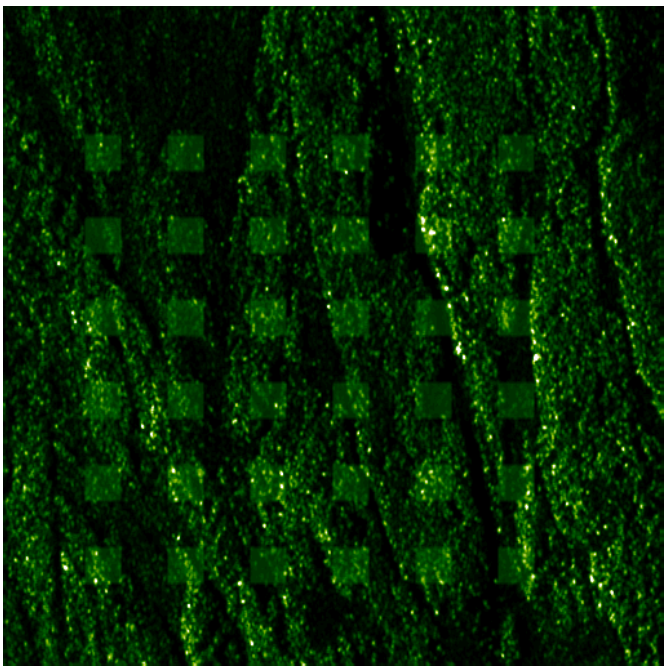

Figure 2. Filtered POLSAR Span Image of the target patch grid.

An estimate of the performance of each statistic can be found by a scheme in the spirit of [7], although the details and assumptions are different. The Bayes error for these statistics is found by using an EM Algorithm for a two-class mixture distribution, which assumes a Gamma PDF after taking the log of the statistic. One initializes the algorithm by choosing a rough estimate for the threshold given as the median plus a dispersion measure for the spread of the data function. This initialization also gives one a rough estimate for the a-prior probabilities since the data set has been partitioned about the threshold. One then estimates the parameters for the Gamma PDF for each class. At this point the EM algorithm is started and for this paper was iterated 10 to 40 times – yielding an estimate for the mixture distribution, including the a-priori and a-posteriori distributions.

TABLE I. BAYES ERROR FOR REAL DATA SIMULATION .

Statistic	Ellipticity	Bartlett	Contrast Ratio
Bayes Error	0.07	0.04	0.04

Plotting the PDF for each class times the a priori probabilities permits an estimate of the threshold that minimizes the total probability of error or Bayes error. Based on this threshold, one estimates the probabilities of error. The Bayes error for each statistic is given in table I.

In addition, a trial-and-error threshold search on the detected image was done for each of the statistics. Since the target mask is known, both the probability of false alarm (PFA) and the probability of detection $P(T > threshold)$ can be determined. For a PFA of 0.01 and 0.1 the probability of detection is shown in table II. The performance of these test statistics is the reverse of what was determined in the ideal simulation. This surprised the first author since it is inconsistent with the simulation results illustrated in figure 1. A heuristic explanation for this dramatic performance turnaround is based on the modeling assumptions. In an actual image, the expected covariance is no longer uniform from pixel-to-pixel. Not only do the pixels vary in intensity, but also in their covariance structure. The estimation of the pixel covariance is essential to all the change statistics; however, the robustness of each change statistic to variations in the covariance estimates is different.

TABLE II. DETECTION PROBABILITY FOR FIXED FALSE ALARM RATE.

Statistic	Threshold	PFA	P(detect)
Ellipticity	1.45	0.1	0.54
Ellipticity	2.45	0.01	0.14
Bartlett	1.02	0.1	0.75
Bartlett	1.8	0.01	0.35
Contrast Ratio	1.85	0.1	0.80
Contrast Ratio	2.65	0.01	0.44

The derivation of the Bartlett test [3], depends upon the LRT and any variation in the estimate of the covariance matrix would appear in the exponential term. So too with the ellipticity, which is also a LRT. Therefore, the total variation induced by the image-to-image variation and the pixel-to-pixel variation appears indirectly in the statistics through the exponential term. However, the contrast ratio is only dependent upon the spectrum of Cxy so there is no amplification of the variations via an exponential term. Hence, the contrast ratio is more robust to these variations, but is also a weaker test under ideal conditions, because it is not tuned to the underlying distributions.

The target locations can be ascertained by using a clustering algorithm. One first creates a detected image where the pixel values are proportional to the a posteriori probabilities. Scaling the X-Y coordinates of the image to one creates a decision space inside a 3D unit cube. The Z-component represents the a-posterior decision probabilities and all the values less than say 0.75 are mapped to zero. The targets appear as cluster near Z=1 plane of the cube. Clustering in this three dimensional space requires an unsupervised algorithm that not only clusters, but also scales the feature space. One algorithm that does both is

the Simultaneous Clustering and Attribute Discrimination algorithm (SCAD2) [8]. A modified version of this is used to cluster the decision space and then the targets are selected from these clusters using a concentration measure, which differentiates between clusters representing dispersed speckle responses and clusters representing concentrated target clusters. This measure is a ratio of the inlier cardinality (points with membership > 0.75) to the cardinality of the cluster. Figure 3 shows eight clusters searching for targets in a decision space containing four target clusters.

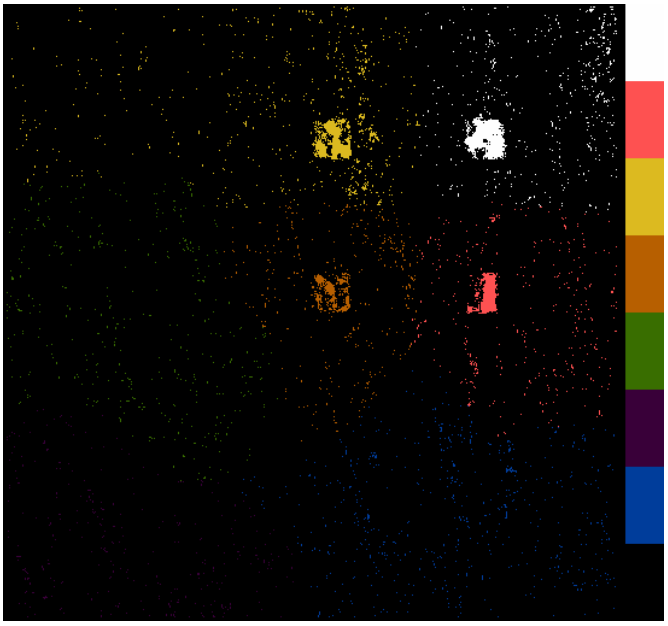

Figure 3. Unsupervised clustering of the decision space with four targets.

The first four clusters represent background regions and the second four clusters represent targets plus some background. The concentration measure easily differentiates the four clusters between targets and background. Note that first cluster (black color) represents the decision points that have be mapped to zero or taken out of consideration. Table III gives the true and actual location of the cluster centers that pass the concentration criterion.

TABLE III. TARGET CLUSTER LOCATION

True X-cood	Cluster X-Coord	True Y-cood	Cluster Y-cood	Probability of Detection
272	274.708	272	275.231	0.853
272	278.039	400	404.324	0.884
400	402.560	272	271.673	0.890
400	401.343	400	403.824	0.917

V. CONCLUSIONS

POLSAR images are constructed from complex radar returns and multi-temporal pairs of these images are used to detect changes in the ground conditions. Three test statistics were studied: the ellipticity, the Bartlett test and the contrast ratio. It was shown that under ideal conditions where the distributions match those assumed in the statistic's derivation, the test statistics are listed in decreasing order of performance. However, when real data is used and the target is injected into one image, the order of performance reverses. It is conjectured that the first two tests, which depend upon the Wishart distribution, are sensitive to the assumptions made on the underlying distribution of the simulation and to the consistency of this assumptions from pixel-to-pixel. The contrast ratio, which is not directly dependent on the distribution of the covariance estimates for each pixel, is more robust to variations in the covariance estimates. Location of the detected targets within the image is determined by using a modified version of a clustering algorithm that determines not only the location of the clusters, but also learns the scale of the individual clusters appearing in the decision space. The concentration of the clusters may then be used to differentiate between interesting targets and background information. These results are a work in progress and more simulation and verification are planned to better quantify these results.

REFERENCES

[1] J-S Lee, M.R. Grunes, T.L. Ainsworth, L-J Du, D.L. Schuler, S. R. Cloude, "Unsupervised classification using polarimetric decomposition and the complex wishart classifier," IEEE TGARS, Vol. 37, No. 5, Sept 1999, pp 2249 –2258.

[2] R. Muirhead, Aspects of Multivariate Statistical Theory, John Wiley, New York, 1982.

[3] K. Conradsen, et. al. "A test statistic in the complex wishart distribution and its application to change detection in polarimetric SAR data," IEEE Trans. Geosci. RemoteSensing, Vol. 41, No. 1, pp. 4-19, Jan, 2003.

[4] S. Jesper, et. al., "CFAR edge detector for polarimetric SAR images," IEEE Trans. Geosci. Remote Sensing, Vol. 41, No. 1, pp. 20-32, Jan, 2003.

[5] F. Hampel, P. Rousseeuw, E. Ronchetti, and W. Stahel, Robust Statistics: The Approach Based on Influence Functions, John Wiley, NY, 1986.

[6] I. Woodhouse, et. al., "Polarimetric interferometry in the Glen Affric Project: results & conclusions," Geoscience and Remote Sensing Symposium, 2002. IGARSS '02, Vol 2, June 2002, pp. 820 – 822.

[7] Y. Bazi, L. Bruzzone, and F. Melgani, "An approach to unsupervised change detection in multitemporal SAR images based on the generalized Gaussian distribution," "Proc. of the IEEE-International Geoscience and Remote Sensing Symposium IGARSS-2004", Anchorage, USA, 20-24 September 2004, vol. 2, pp. 1402-1405.

[8] H. Frigui, and O. Nasraui, "Unsupervised learning of prototypes and attribute weights," Pattern Recognition, 37 (2004) pp. 567-581.